Supplementary Information

Simultaneous improvement in flame resistance and thermal conductivity of epoxy/Al_2O_3 composites by incorporating polymeric flame retardant-functionalized graphene

Yuezhan Feng[a], Ji Hu[a], Yang Xue[a], Chengen He[a], Xingping Zhou[a*], Xiaolin Xie[ab], Yunsheng Ye [a*], Yiu-Wing Mai[c]

[a] *Key Laboratory of Material Chemistry for Energy Conversion and Storage (HUST), Ministry of Education, School of Chemistry and Chemical Engineering, Huazhong University of Science and Technology, Wuhan 430074, China.*

[b] *State Key Laboratory of Material Processing and Die & Mould Technology, Huazhong University of Science and Technology Wuhan 430074, China*

[c] *Centre for Advanced Materials Technology (CAMT), School of Aerospace, Mechanical and Mechatronic Engineering J07, The University of Sydney, Sydney, NSW 2006, Australia.*

Preparation of graphene oxide (GO)

Graphene oxide (GO) was chemically exfoliated from natural graphite by the modified Hummers' method. Typically, 10 g graphite powder and 5 g $NaNO_3$ were dispersed in 230 mL concentrated H_2SO_4 (98%) with mechanical stirring and ice-bath treatment for 30 min. Then 30 g $KMnO_4$ was slowly added into the above system within 1 h, followed by continuous stirring for 2 h with the temperature of the system being controlled below 10 ^oC by an ice-bath. Subsequently, the system was transferred to an oil bath with vigorous stirring at 35 ^oC for 2 h. After which, 460 mL deionized water was added dropwise into the reaction system and the temperature was simultaneously raised to 95 ^oC for 15 min. Finally, the reaction solution was poured into a 2 L beaker with 700 mL deionized water to terminate the oxidation reaction. Next 50 mL H_2O_2

was added dropwise into the solution with hand stirring. The resultant GO solution was allowed to stand overnight. The supernatant was poured off and 500 mL 5% HCl aqueous solution (repeating at least 3 times) or water was added to remove foreign ions. The residual foreign ions were further removed by dialysis for at least 5 days until the pH≥5. At last, the obtained GO aqueous solution was freeze-dried into a spongelike solid to reserve.

Characterization of PDMPD and PFR-*f*RGO.

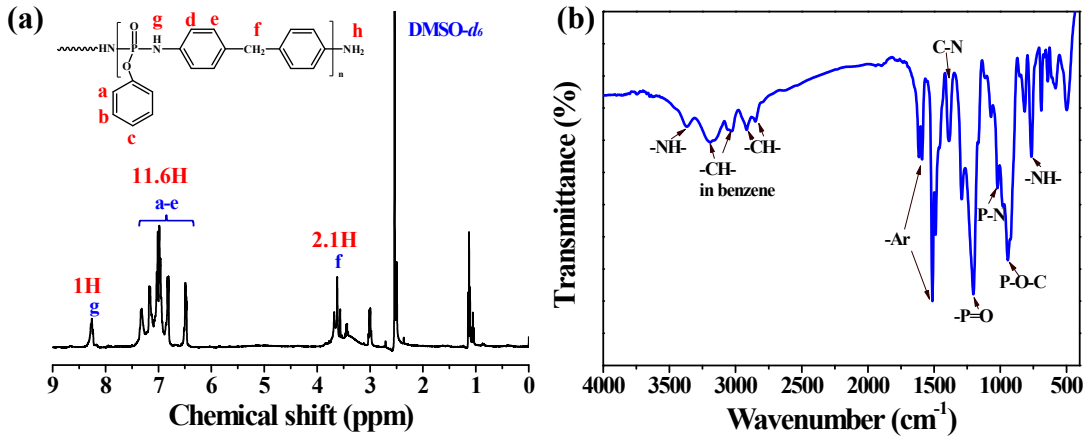

Figure S1. (a) H^1 NMR and (b) FTIR spectra of PDMPD.

The chemical structures of PDMPD were characterized by H^1 NMR and FTIR. The expected characteristic peaks of H (Figure S1a), including 8.25 ppm (-NH-, 1H), 7.5-6.5 ppm (benzene ring, 12H), 3.6 ppm ($-CH_2-$, 2H) and 3.0 ppm (terminal $-NH_2$), are observed on the H^1 NMR spectrum of PDMPD. Moreover, the FTIR absorption peaks of characteristic groups (Figure S1b), such as N-H stretching vibration at 3373 cm^{-1}, C-H stretching vibrations at 3192, 3031, 2920 cm^{-1}, skeletal vibrations of phenyl at 1614, 1512 cm^{-1}, C-N stretching vibration at 1387 cm^{-1}, P=O stretching vibration at 1200 cm^{-1}, P-N stretching vibration at 1020 cm^{-1}, and P-O-C stretching vibration at 943 cm^{-1} are found in the FTIR spectrum of PDMPD. These results are consistent with the previous literature,[1] suggesting the successful synthesis of polymeric flame retardant.

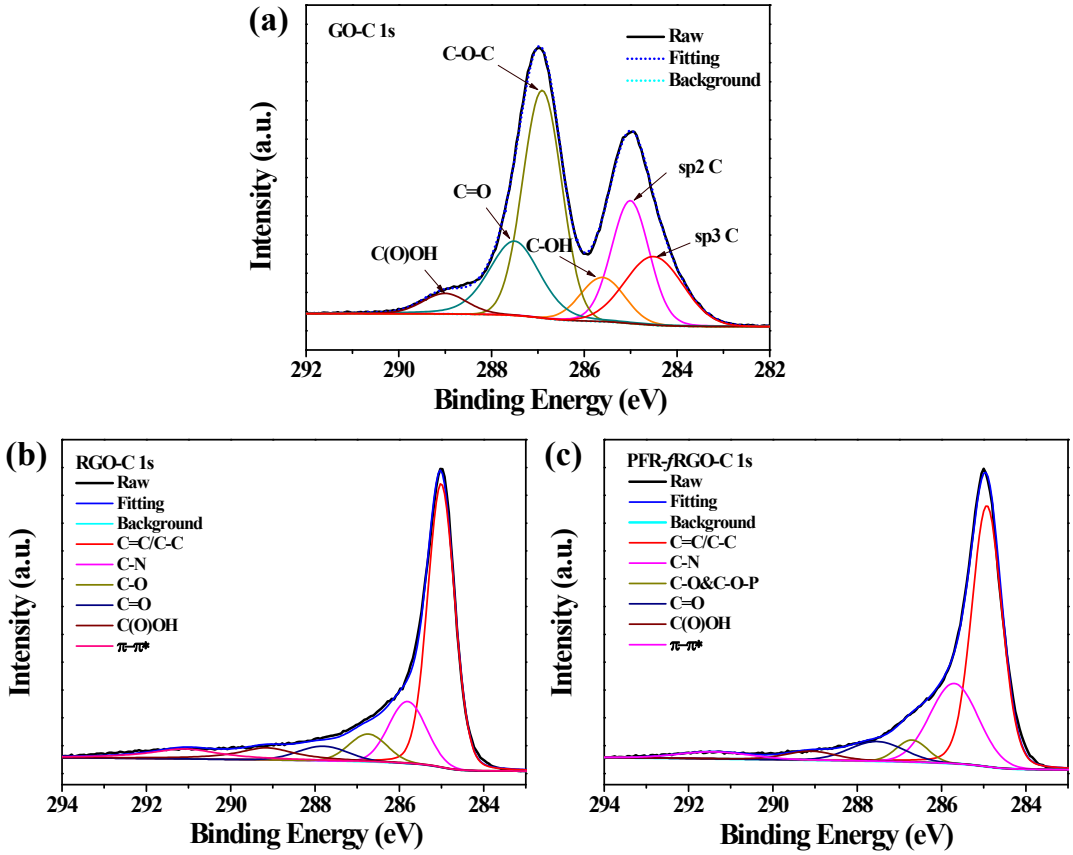

Figure S2. High-resolution C 1s XPS spectra of (a) GO, (b) RGO and (c) PFR-*f*RGO.

Density measurements

Density measurements based on buoyancy method (Archimedes' principle) were performed on a METTLER-TOLEDO analytical balance with a density determination kit. The density of a solid is determined with the aid of a liquid whose density ρ_0 is known (water in this work, ρ_0=1.0 g/cm^3). The solid is weighed in air (m_A) and then in the auxiliary liquid (m_B). The solid density ρ can be calculated from the two weighings as follows:

$$\rho = \frac{m_A}{m_A - m_B}(\rho_0 - \rho_a) + \rho_a \qquad (1)$$

where ρ_a is the air density (0.0012 g/cm^3).

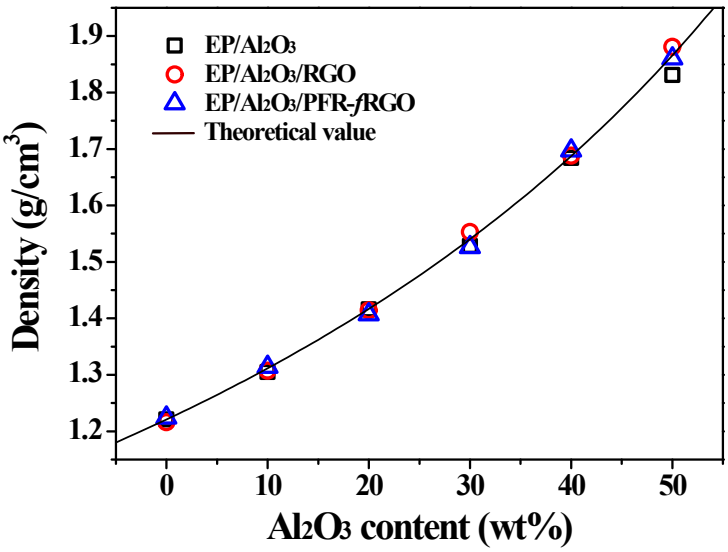

Figure S3. Experimental (dots) and theoretical (line) densities of epoxy composites.

The theoretical density was estimated by Rules of Mixtures based on the assumption of ideal without defects:[2]

$$\rho = \sum_{i=1}^{n} f_i \rho_i = 1 \Big/ \sum_{i=1}^{n} \frac{m_i}{\rho_i} \qquad (2)$$

where ρ is the density of composite, ρ_i is the densities of components, f_i and m_i are the volume and mass fractions of components, respectively. In this work, the densities of matrix, Al_2O_3 and graphene are 1.221, 3.95 and 1.06 g/cm^3, respectively.[3] The results of the experimental and theoretical densities are shown in Figure S3.

XRD analyses of epoxy composites

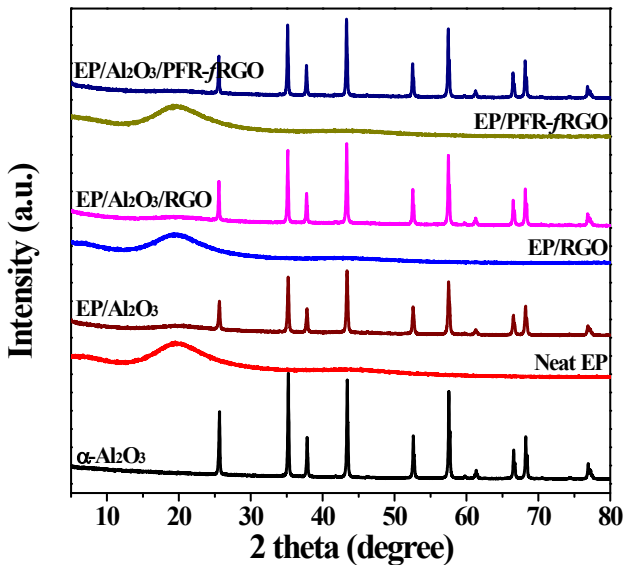

Figure S4. XRD spectra of α-Al_2O_3 and epoxy composites.

Morphology of epoxy-based composites

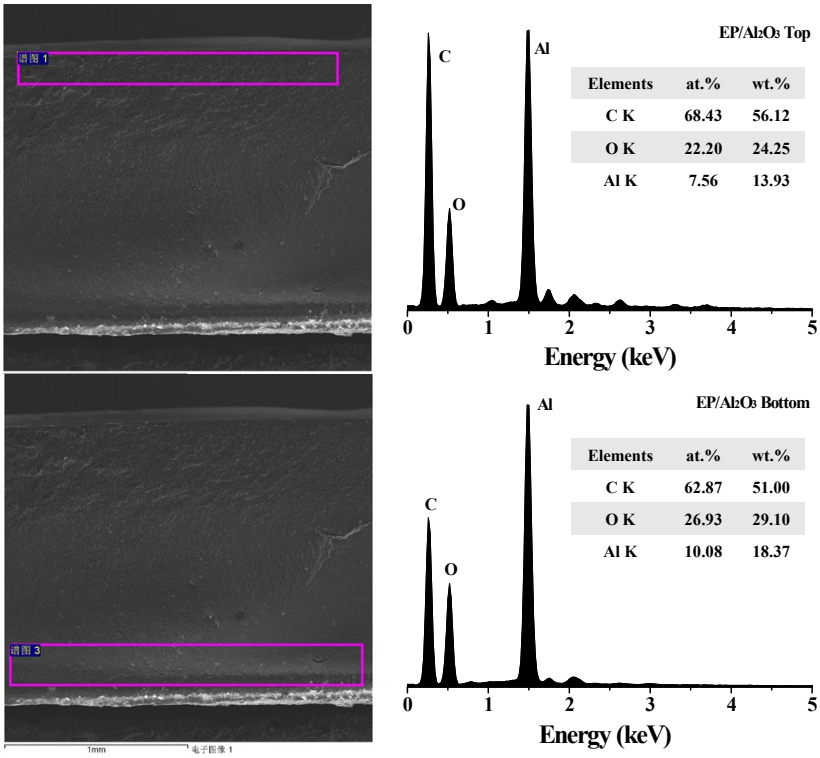

Figure S5. SEM images and EDX spectra of EP/Al_2O_3 at top and bottom regions.

The settlement characteristics of microparticles under the gravity action is noteworthy during curing process due to the low viscosity of epoxy and poor interfacial interaction between Al_2O_3 and epoxy, which leads to a lower filler loading relative to the whole at top region. As shown in Figure S5, the EDX spectra show that the Al element content at bottom is higher than that at top, which confirms the settlement characteristics of Al_2O_3 in EP/Al_2O_3 composites. The introduction of graphene was expected to increase the viscosity of epoxy by forming 3D network structure, which further weakened the settlement action of Al_2O_3. In fact, as shown in Figure S6 and S7, the Al element contents are almost consistent in the top and bottom region, suggesting a uniform distribution of Al_2O_3 in epoxy, which is favour of the thermal conductivity of composites.

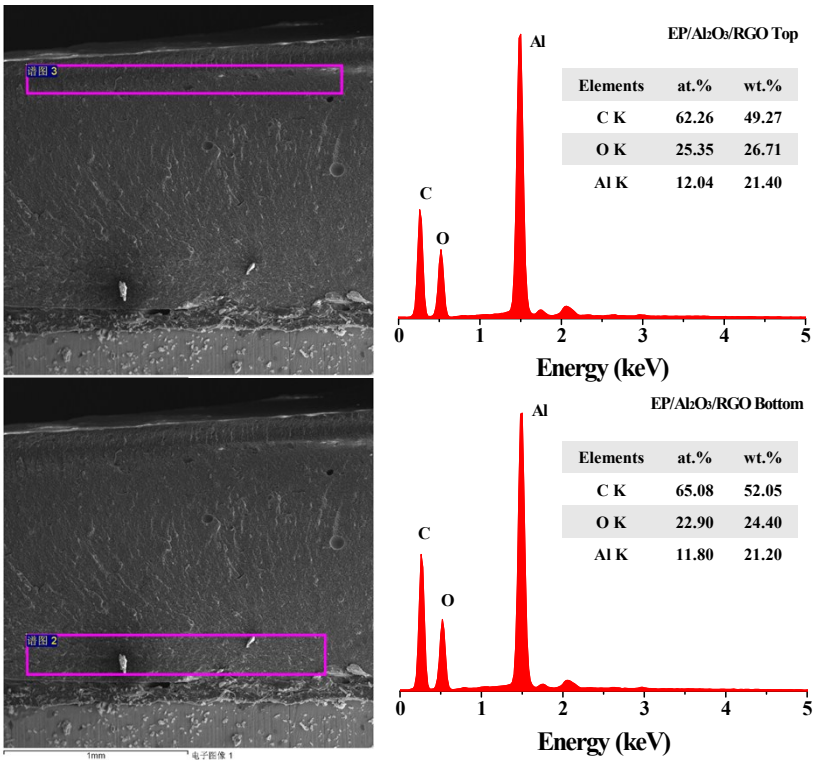

Figure S6. SEM images and EDX spectra of EP/Al_2O_3/RGO at top and bottom regions.

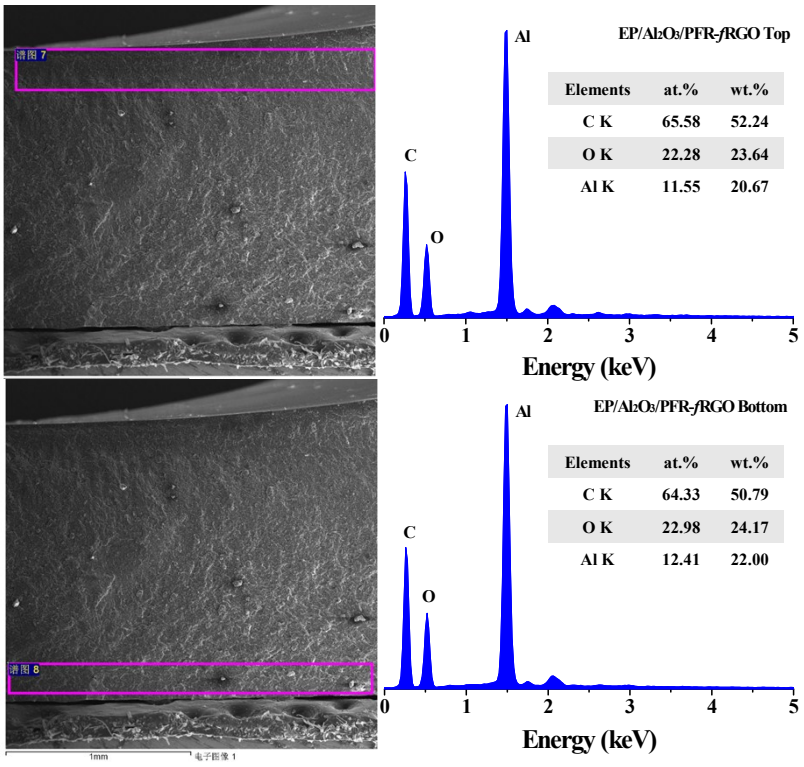

Figure S7. SEM images and EDX spectra of EP/Al_2O_3/PFR-*f*RGO at top and bottom regions.

Mechanical properties of epoxy-based composites

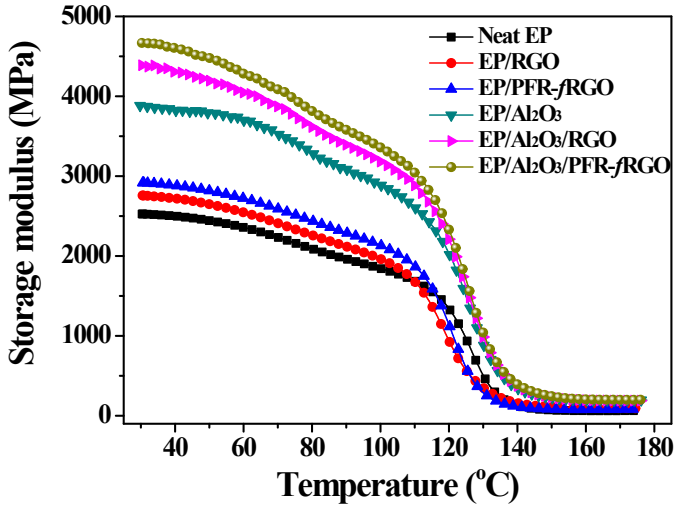

Figure S8. Storage modulus of neat EP, EP/RGO, EP/PFR-*f*RGO, EP/Al_2O_3, EP/Al_2O_3/RGO and EP/Al_2O_3/PFR-*f*RGO composites with 50 wt% Al_2O_3 particles and 1 wt% graphene.

Dynamic mechanical analyses (DMA) of EP/graphene composites were carried out on a TA Instruments Q800 DMA in single cantilever beam mode with an oscillatory frequency of 1 Hz, to confirm the change of storage modulus of epoxy and EP/Al_2O_3 by the introduced graphene. As shown in Figure S8, incorporating a large amount of Al_2O_3 particles (50 wt%) into epoxy results in the significant increase of the storage modulus below the glass-transition temperature (T_g), which are further improved by adding graphene due to the immobilization effect of Al_2O_3 and graphene for polymer chains. Moreover, flame retardant functionalization for graphene can effectively perfect the interfacial bonding, resulting in a higher storage modulus.

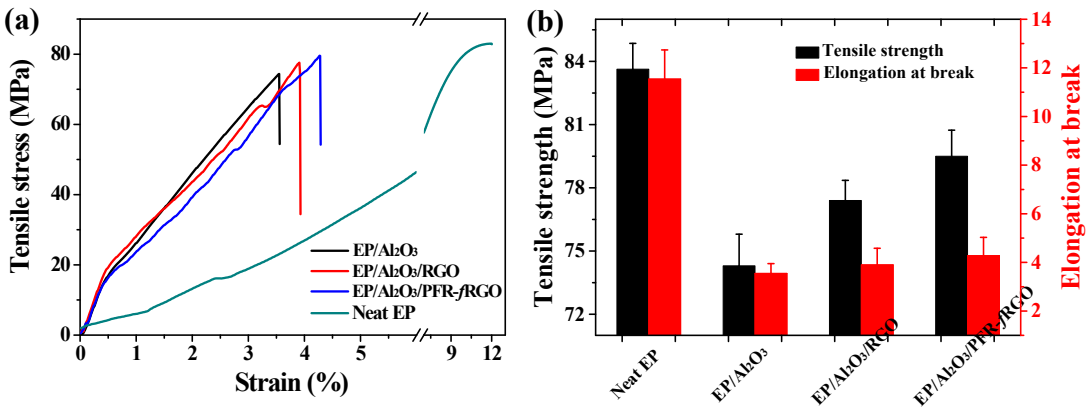

Figure S9. (a) Stress-strain curves and (b) tensile property parameters of neat EP,

EP/Al_2O_3, EP/Al_2O_3/RGO and EP/Al_2O_3/PFR-*f*RGO composites with 50 wt% Al_2O_3 particles and 1 wt% graphene.

Tensile testing was performed by using a SUNS UTM2203 universal tensile testing machine at a crosshead rate of 10 mm/min according to the standard GB/T 1040-2006. Figure S9 shows the typical stress-strain curves and tensile properties of neat EP, EP/Al_2O_3, EP/Al_2O_3/RGO and EP/Al_2O_3/PFR-*f*RGO composites with 50 wt% Al_2O_3 particles and 1 wt% graphene. As a hard but brittle polymer, epoxy resin presents a high tensile strength of 83.6 MPa but a low elongation at break of 11.5% (low tensile toughness). Incorporating 50 wt% Al_2O_3 particles into epoxy matrix leads to the decrease of both strength and toughness due to the poor interfacial interaction and serious agglomeration behavior. Adding 1 wt% graphene into EP/Al_2O_3 composite is able to effectively improve the dispersion (Figure S6 and S7) and interfacial adhesion (Fig. 3e and 3f) of Al_2O_3 particles in EP matrix, further resulting in the increase of tensile strength and toughness (Figure S9).

Thermal conductivity of epoxy-based composites

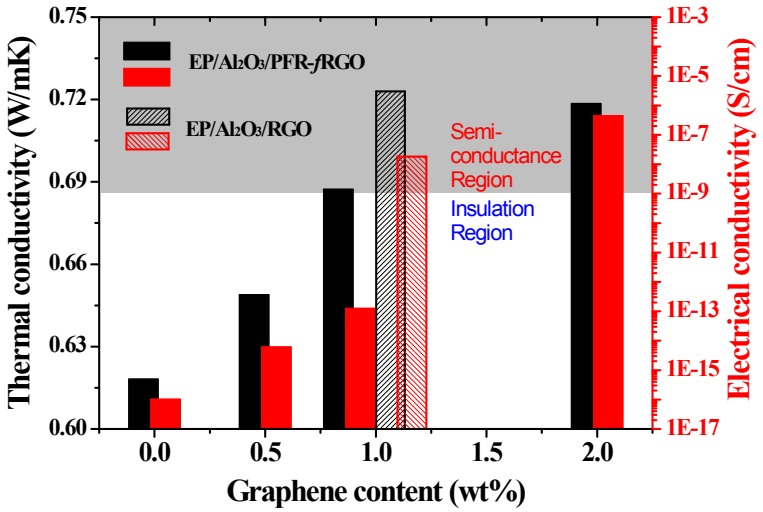

Figure S10. Thermal and electrical conductivity as a function of graphene content for EP/Al_2O_3/graphene composites with 50 wt% Al_2O_3 particles.

Figure S10 shows the thermal and electrical conductivity as a function of graphene content for EP/Al_2O_3/graphene composites with 50 wt% Al_2O_3 particles. The thermal conductivity values of composites exhibit a continuous increase as a function of

graphene loading within testing range due to more conduction paths formed by the adding graphene.

The volume electrical conductivity measurements were performed on a PC40B digital resistance tester (Shanghai Anbiao Electronics Co., Ltd. China) according to the standard GB/T 1410-2006. The disc-like samples were 100 mm in diameter and 2 mm in thickness, and the applied voltage to the sample was fixed at 500 V. As shown in Figure S8, the electrical conductivity of composites improves remarkably with the increase of graphene content, and a sharp increase was observed between 1 and 2 wt% PFR-*f*RGO, which means a percolation threshold behavior happened, i.e., forming a conductive network during this loading range. Moreover, the composite containing RGO shows a higher electrical conductivity compared to the PFR-*f*RGO composite, which was ascribed to the barrier effect for electronic transmission by the coating of flame retardant (PDMPD) chains. Taking into account the thermal and electrical conductivity, the composites with 1 wt% PFR-*f*RGO were believed to meet the requirement of electric insulation and thermal conductivity for electronic packaging materials.

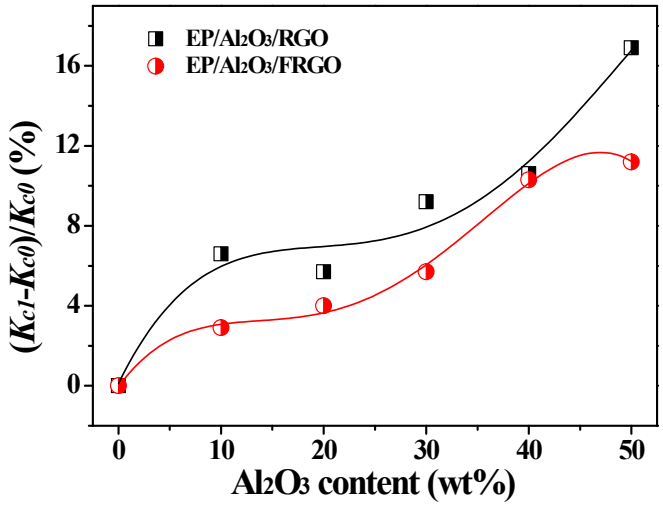

Figure S11. The synergistic effect strength of graphene and Al_2O_3 as a function of Al_2O_3 content.

The strength of the synergistic effect is defined as $(K_{c1}-K_{c0})/K_{c0}$,[4] where K_{c1} is the thermal conductivity of EP/Al_2O_3/RGO or EP/Al_2O_3/PFR-*f*RGO, K_{c0} is the thermal conductivity of EP/Al_2O_3.

Morphology and size of α-Al_2O_3

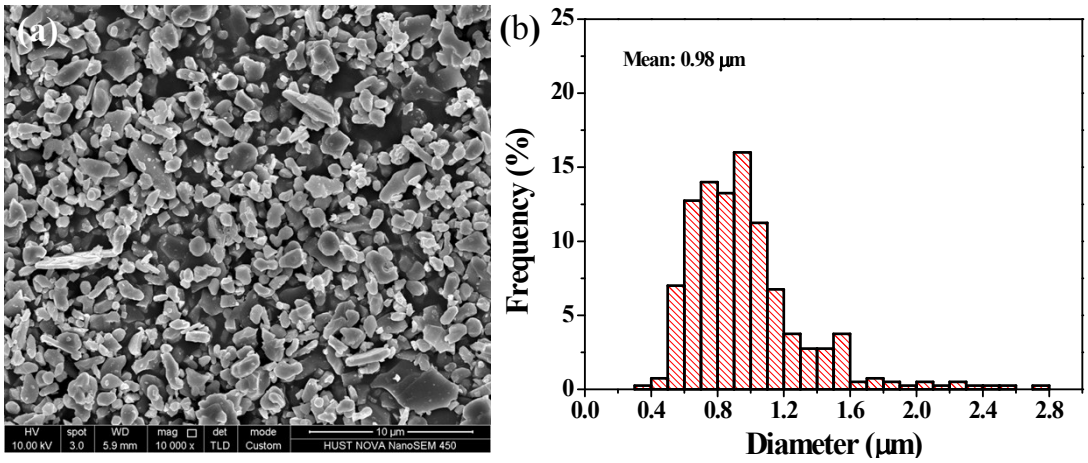

Figure S12. (a) SEM image and (b) particle size distribution of α-Al_2O_3 particles.

Figure S12 is the SEM image and particle size distribution of α-Al_2O_3 particles. The KPJ01 α-Al_2O_3 exhibits an irregular shape with a relatively homogeneous size. For convenience, the irregular α-Al_2O_3 were regarded as spherical particles in our model-fitting process. The mean diameter of α-Al_2O_3 is calculated based on the statistical data of particles size by Nano Measurer 1.2 software from Figure S12a, and the result was shown in Figure S12b. The obtained mean diameter of α-Al_2O_3 is 0.98 μm, which is well agreement with the product information given by manufacturer (D50=1.1μm).

Char analyses

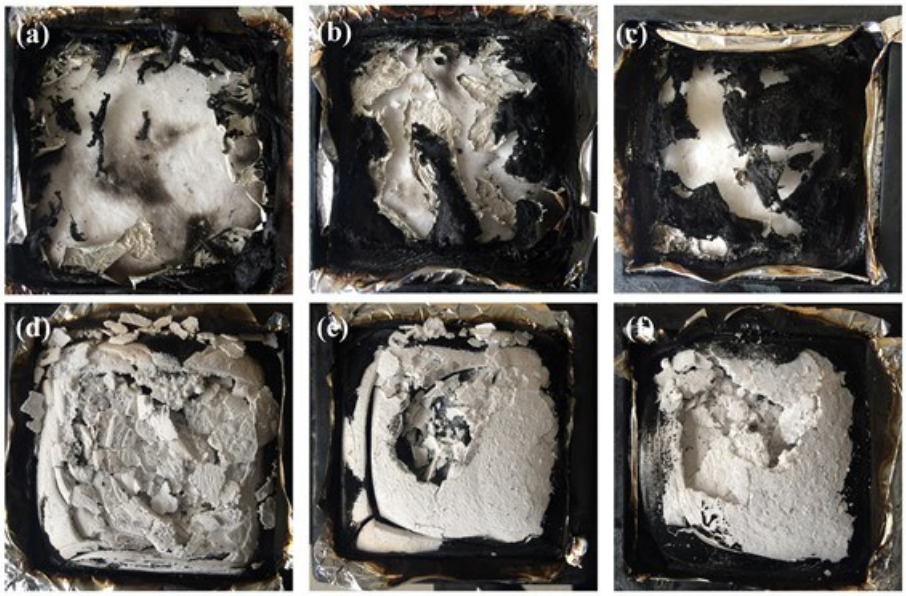

Figure S13. Digital photos of the residues after cone test of (a) neat EP, (b) EP/RGO, (c) EP/PFR-*f*RGO, (d) EP/Al_2O_3, (e) EP/Al_2O_3/RGO and (f) EP/Al_2O_3/PFR-*f*RGO.

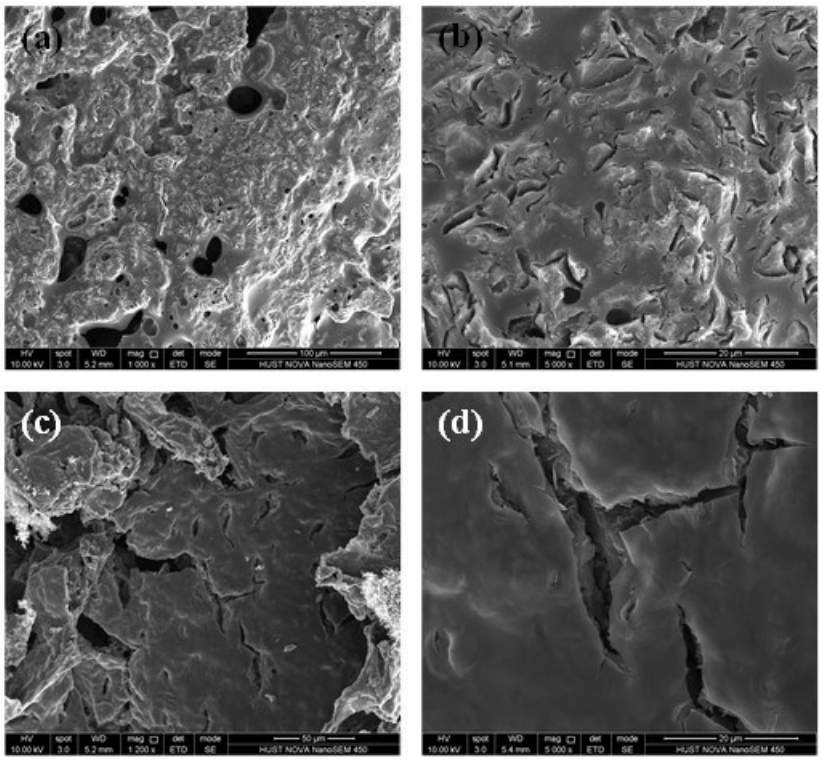

Figure S14. SEM images the residues after cone test with different magnification of (a, b) EP/RGO and (c, d) EP/PFR-*f*RGO composites

References

1. Q. Tai, Y. Hu, R. K. K. Yuen, L. Song and H. Lu, *J. Mater. Chem.*, 2011, **21**, 6621-6627.
2. S. Duwe, C. Arlt, S. Aranda, U. Riedel and G. Ziegmann, *Compos. Sci. Technol.*, 2012, **72**, 1324-1330.
3. M. A. Rafiee, R. Javad, W. Zhou, S. Huaihe, Y. Zhong-Zhen and K. Nikhil, *ACS Nano*, 2009, **3**, 3884-3890.
4. A. Yu, P. Ramesh, X. Sun, E. Bekyarova, M. E. Itkis and R. C. Haddon, *Adv. Mater.*, 2008, **20**, 4740-4744.